



CHORUS

This is the accepted manuscript made available via CHORUS. The article has been published as:

Mutual projectile and target ionization in 1-MeV/amu $N^{\{4+\}}$ and $N^{\{5+\}}$ +He collisions

X. Wang, K. Schneider, A. Kelkar, M. Schulz, B. Najjari, A. Voitkiv, M. Gundmundsson, M. Grieser, C. Krantz, M. Lestinsky, A. Wolf, S. Hagmann, R. Moshhammer, J. Ullrich, and D. Fischer

Phys. Rev. A **84**, 022707 — Published 16 August 2011

DOI: [10.1103/PhysRevA.84.022707](https://doi.org/10.1103/PhysRevA.84.022707)

Mutual Projectile and Target Ionization in 1 MeV/amu N^{4+} and N^{5+} +He Collisions

X. Wang^{1,2,3,4}, K. Schneider^{1,2}, A. Kelkar^{1,2}, M. Schulz⁵, B. Najjari¹, A. Voitkiv¹, M. Gundmundsson⁶, M. Grieser¹, C. Krantz¹, O. Novotny¹, M. Lestinsky^{1,7}, A. Wolf¹, S. Hagmann⁷, R. Moshhammer¹, J. Ullrich¹, and D. Fischer^{1*}

¹*Max-Planck-Institut für Kernphysik, Saupfercheckweg 1, 69117 Heidelberg, Germany*

²*Extreme Matter Institute EMMI, GSI Helmholtzzentrum für*

Schwerionenforschung GmbH, Planckstraße 1, 64291 Darmstadt, Germany

³*Shanghai EBIT Laboratory, Institute of Modern Physics, Fudan University, Shanghai 200433, China*

⁴*The Key Laboratory of Applied Ion Beam Physics, Ministry of Education, China*

⁵*Physics Department and LAMOR, University of Missouri-Rolla, Rolla, Missouri 65409, USA*

⁶*Stockholm University, Atomic Physics, Alba Nova, S-106 91 Stockholm, Sweden and*

⁷*GSI Helmholtzzentrum für Schwerionenforschung GmbH, Planckstraße 1, 64291 Darmstadt, Germany*

We have studied Mutual Projectile and Target Ionization (MPTI) in 1MeV/amu N^{4+} and N^{5+} +He collisions in kinematically complete experiments by measuring the momenta of the recoil ion and both ejected electrons in coincidence with the charge-changed projectiles. By means of four-particle Dalitz (4-D) plots, in which multiple differential cross sections are presented as a function of the momenta of all four particles, experimental spectra are compared with theoretical results from various models. The experimental data are qualitatively reproduced by higher-order calculations, where good agreement is achieved for N^{5+} +He collisions, while some discrepancies persist for N^{4+} +He collisions.

PACS numbers:

I. INTRODUCTION

The understanding of few-body correlated quantum dynamics is a fundamental problem in atomic physics and beyond. Here, the study of mutual projectile and target ionization (MPTI) is of particular interest [1–7], since it is one of the simplest systems where only four particles are actively involved, providing insight into the ionization process of both collision partners. Several "reaction channels" represented by transition matrix elements in a perturbative description contribute to MPTI. In one the two active electrons are ejected by directly interacting with each other (e-e channel). In perturbation theory, this mechanism corresponds to the first order term. A second channel proceeds through independent interactions between the electron of one collision partner and the core of the other (referred to as n-e channel), which is a higher-order mechanism. The e-e channel attracted considerable attention, because a relatively weakly bound target electron can be viewed as quasi-free, hence the electron emission from the projectile is analog to electron-impact ionization of the projectile (known as an (e,2e) reaction [8, 9]). It is thus possible to study (e,2e) dynamics for ionic targets in ion-atom collision experiments in an approximate manner [4]. Direct (e,2e) measurements (i.e. using truly free electron beams) with ionic targets are extremely difficult and multiple differential data are currently not available.

Regarding the electron ejection from the projectile, the e-e channel is also termed anti-screening ionization [10]. This mechanism exhibits a threshold (to which we refer as the anti-screening threshold) because in the rest frame of the projectile the target electron must have a kinetic energy which is larger than the ionization potential of the projectile. Small perturbations η (projectile charge to speed ratio) normally correspond to projectile energies well above this threshold. Here the e-e channel is expected to be more important because the collision time is too short, i.e. the perturbation too small, for two independent transitions of the active electrons to occur with significant probability. Accordingly, the higher-order reaction channels are expected to become more important with increasing η . For close to or below threshold systems, the e-e channel is strongly suppressed, if present at all.

One important question relates to the respective importance of the first- and higher-order mechanisms (or in other words the e-e and n-e channels, respectively) and to what extent they can be separated from each other, e.g. via monitoring the momentum balance between the collision partners exploiting experimental techniques like cold target recoil-ion momentum spectroscopy (COLTRIMS) or Reaction Microscopes. Under certain kinematical conditions, the experimental data allows for such a separation by analyzing the momentum transferred to the recoil ion, as for the e-e channel the recoiling ion is essentially passive so that the momentum transferred to it is significantly smaller than in the n-e channel [2, 3]. Furthermore, one can attribute a pronounced angular correlation between the two ejected electrons to the e-e channel, while an angular correlation between the electron ejected from one collision partner and

* E-mail: fischer@mpi-hd.mpg.de

the core of the other, is indicative for the n-e reaction [4]. However, the former method requires a relatively large absolute difference in the momentum transfer to the recoiling ion between the n-e and e-e channels. Regarding the latter method Ferger et. al. [5] have shown that for each collision partner the correlation between the electron and the core to which it is initially bound (i.e. the Compton profile of the initial ground state) could completely mask the angular correlation pattern resulting from the collision.

In this work we report an alternative, and as it turns out a very powerful approach to separate various reaction channels. To this end we have studied MPTI in collisions both well above the threshold (1MeV/amu $N^{4+} + He$), and close to threshold (1MeV/amu $N^{5+} + He$) for MPTI. The experimental data is presented in terms of four-particle Dalitz (4-D) plots and compared to various theoretical models. As we will show, in this representation the e-e and n-e channels can be well separated. Dalitz plots were initially introduced to analyze three-body reactions in particle physics [11]. More recently, this technique has been applied to analyze atomic fragmentation dynamics [12] and generalized to four-body processes like MPTI or double ionization [13–15]. It was demonstrated that this method is able to give rich information about the collision dynamics, and even new collision mechanisms could be identified [14].

II. EXPERIMENT

The experiment was performed at the test storage ring (TSR) [16] of the Max-Planck-Institut für Kernphysik (MPI-K) in Heidelberg. The TSR is excellently suited for ion-atomic collision studies with Reaction Microscopes. Ultra high vacuum (10^{-11} mbar) ensures low-background conditions and long storage times and high beam intensity of up to a few $10\mu A$ can be readily achieved. The ion beams are cooled [17] by means of the electron cooling mechanism, and beam sizes below 1mm were obtained. The ion beams were intersected with a cold ($T \leq 2K$) supersonic gas jet of helium with a density of about 10^{11} atoms/cm³.

The ionized projectiles were charge-to-mass ratio selected by a dipole magnet and then detected by a scintillator detector [18]. A fast timing signal from the projectile detector served as a start signal for a coincidence setup with all other collision fragments. The ejected electrons and recoil ions were extracted by a weak electric field ($E \approx 10$ V/cm) along the longitudinal direction (z direction, defined by the incoming beam direction) and detected by two-dimensional position-sensitive channel-plate detectors. The electron detector was located downstream from the target region (i.e. electrons were detected in the forward direction), and a uniform magnetic field of 10G, directed at an angle of about 12 degree with respect to z direction, guided electrons with a transverse momentum of less than 1.5 au onto the detector. During the time of beam injection into the TSR, the electron detector was moved several cm away from the beam axis and moved back in position again when the beam had been cooled down. A delay line anode operating in multi-hit mode, could detect both electrons simultaneously.

The recoil ions and both electrons were fully momentum analyzed using a standard Reaction Microscope [19–22]. It is straightforward to get the momenta of the projectile by using momentum conservation. It should be noted that in the following electrons with larger forward velocity are assumed to be emitted from the projectile, whereas the electrons with smaller longitudinal momentum are assigned to the target. This is reasonable as the projectile has a velocity of 6.33 au in the forward direction while the target is practically at rest.

III. THEORY

We adopt the semi-classical treatment and assume that the target nucleus, having a charge Z_A , is at rest and taken as the origin. In the frame of the nucleus of the target the projectile nucleus with a charge Z_I ($Z_I \gg 1$) moves along a straight-line classical trajectory $\mathbf{R}(t) = \mathbf{b} + \mathbf{v}t$, where \mathbf{b} is the impact parameter, \mathbf{v} is the projectile velocity.

For simplicity we shall consider that the target has only one (active) electron. As before, we denote the coordinates of the electron of the target and that of the projectile, given with respect to the target nucleus, by $\boldsymbol{\rho}$ and \mathbf{s} , respectively, and $\boldsymbol{\xi}$ and \mathbf{r} are the coordinates of the target and projectile electrons with respect to the projectile nucleus [see Fig. 1].

The electronic wavefunction of the colliding particles is described by the Schrödinger equation:

$$\left(i\frac{\partial}{\partial t} - H_I - H_A - V\right)\Psi(\mathbf{r}, \boldsymbol{\rho}, t) = 0. \quad (1)$$

Here H_I and H_A are the electronic Hamiltonians of the projectile ion and the atomic target, respectively,

$$V = \frac{Z_I Z_A}{R(t)} - \frac{Z_A}{s} - \frac{Z_I}{|\boldsymbol{\rho} - \mathbf{R}(t)|} + \frac{1}{|\mathbf{s} - \boldsymbol{\rho}|}. \quad (2)$$

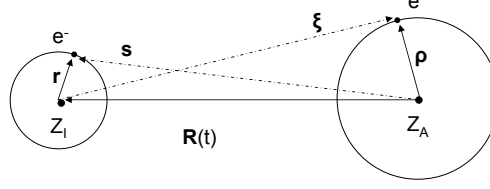


FIG. 1: Schematic illustration of the coordinate system of the projectile-target collision.

The prior form of the semiclassical transition amplitude is given by

$$a_{fi}(\mathbf{b}) = i \int_{-\infty}^{+\infty} dt \langle \Psi_f^{(-)}(t) | (\hat{H} - i \frac{\partial}{\partial t}) | \Phi_i(t) \rangle. \quad (3)$$

In (3) $\Psi_f^{(-)}(t)$ is the solution of the full Schrödinger equation and $\Phi_i(t)$ is the solution of

$$i \frac{\partial \Phi_i}{\partial t} = (\hat{H}_A + \hat{H}_I + \hat{W}(t)) \Phi_i \quad (4)$$

where $\hat{W}(t)$ is a distortion potential.

The transition amplitude (3) can be converted into the momentum space by performing the Fourier transformation

$$S_{fi}(\mathbf{q}_\perp) = \frac{1}{2\pi} \int d^2\mathbf{b} a_{fi}(\mathbf{b}) \exp(i\mathbf{q}_\perp \cdot \mathbf{b}). \quad (5)$$

The quantity \mathbf{q}_\perp then can be thought of as the two-dimensional transverse ($\mathbf{q}_\perp \cdot \mathbf{v} = 0$) momentum transfer to the target. Using the amplitude (5) the cross section for MPTI, differential in the momenta of the emitted electrons, is written as

$$\frac{d^6\sigma}{d\mathbf{k}d\boldsymbol{\kappa}d\mathbf{q}_\perp} = \int d^2\mathbf{q}_\perp |S_{fi}(\mathbf{q}_\perp)|^2 \quad (6)$$

where \mathbf{k} is the momentum of the projectile electron in the projectile rest frame and $\boldsymbol{\kappa}$ is the momentum of the target electron in the target rest frame.

As a first attempt to describe the MPTI we shall use the first order perturbative treatment (FBA) [23, 24]. In this approach the electronic wave functions $\Phi_i(t)$ and $\Psi_f^{(-)}$ are given by:

$$\Phi_i^{FBA}(t) = u_0(\boldsymbol{\rho}) e^{-i\epsilon_0 t} \psi_0(\mathbf{s} - \mathbf{R}) e^{-i\epsilon_0 t} e^{i(\mathbf{v} \cdot \mathbf{s} - i \frac{v^2}{2} t)} \quad (7)$$

and

$$\Psi_f^{FBA}(t) = u_f^{(-)}(\boldsymbol{\rho}) e^{-i\epsilon_f t} \psi_f^{(-)}(\mathbf{s} - \mathbf{R}) e^{-i\epsilon_f t} e^{i(\mathbf{v} \cdot \mathbf{s} - i \frac{v^2}{2} t)} \quad (8)$$

u_0 and $u_f^{(-)}$ are the initial and final electronic states of the target respectively, given in the target frame. ψ_0 and $\psi_f^{(-)}$ describe the initial and final internal states of the projectile given in the projectile rest frame. Further $\epsilon_{0(f)}$ and $\epsilon_{0(f)}$ are the initial (final) electron energies in the internal states of the projectile and target respectively. Each energy is given in the rest frame of corresponding parent center.

Using Eqs. 3-5 one can show that the first order transition amplitude in the momentum space reads

$$\begin{aligned} S^{FBA}(\mathbf{q}_\perp) &= \frac{1}{2\pi} \int d\mathbf{b} e^{i\mathbf{q}_\perp \cdot \mathbf{b}} a_{fi}^{FBA}(\mathbf{b}) \\ &= \frac{2i \langle u_f^{(-)} | e^{-i\mathbf{q} \cdot \boldsymbol{\rho}} | u_0 \rangle \langle \psi_f^{(-)} | e^{i\mathbf{q} \cdot \mathbf{r}} | \psi_0 \rangle}{v q^2} \end{aligned}$$

where $\mathbf{q} = (\mathbf{q}_\perp, q_{min} = (\epsilon_f - \epsilon_0 + \epsilon_f - \epsilon_0)/v)$ is the momentum transfer to the target system.

The first order approximation is expected to represent a good tool for the collision system only provided the conditions $Z_I/v \ll 1$ and $Z_A/v \ll 1$ are fulfilled. In order to treat MPTI, in which the ratio Z_I/v may be not small we take the initial and final states as

$$\Phi_i^{EA}(t) = L_i(\boldsymbol{\xi})\Phi_i^{FBA}(t) \quad (9)$$

$$\Psi_f^{EA}(t) = L_f(\boldsymbol{\xi})\Psi_f^{FBA}(t) \quad (10)$$

where L_i and L_f are the distortion factors which, according to the symmetric eikonal approximation (EA), are given by

$$L_i = (v\xi + \mathbf{v} \cdot \boldsymbol{\xi})^{-i\nu} \quad (11)$$

$$L_f = (v\xi - \mathbf{v} \cdot \boldsymbol{\xi})^{i\nu} \quad (12)$$

with $\nu = \frac{Z_I}{v}$. The corresponding transition amplitude in the momentum space reads

$$S_{fi}(\mathbf{q}_\perp) = - \frac{2i}{v^{1+2i\nu}} \int d^2\mathbf{p}_\perp f(p_\perp, \nu) \langle \psi_n(\mathbf{r}) | \exp(i(\mathbf{p}_\perp - \mathbf{q}) \cdot \mathbf{r}) | \psi_0(\mathbf{r}) \rangle \\ \times \frac{1}{|\mathbf{q} - \mathbf{p}_\perp|^2} \langle u_m(\boldsymbol{\rho}) | Z_A \exp(i\mathbf{p}_\perp \cdot \boldsymbol{\rho}) - \exp(i\mathbf{q} \cdot \boldsymbol{\rho}) | u_0(\boldsymbol{\rho}) \rangle \quad (13)$$

where the function $f(p_\perp, \nu)$ is defined according to

$$f(p_\perp, \nu) = \lim_{\alpha \rightarrow +0} \lim_{\zeta \rightarrow +0} \frac{\Gamma(1 - i\nu)\Gamma(1/2 + i\nu)}{2\pi\Gamma(1/2)\Gamma(2i\nu)} p_\perp^{\alpha-2+2i\nu} \exp(-\zeta p_\perp) \quad (14)$$

where $\Gamma(x)$ is the gamma-function and the integration is performed over the two-dimensional transverse vector \mathbf{p}_\perp ($\mathbf{p}_\perp \cdot \mathbf{v} = 0$).

Finally, we calculated MPTI cross sections within an independent electron model, termed as TS-2. It is modelled as single ionization of the target occurring simultaneously but independently with electron loss from the projectile. These TS-2 cross sections were calculated by convoluting target ionization and projectile loss cross sections, using the same method as in [14].

IV. RESULTS AND DISCUSSION

The 4-particle momentum balance is displayed in 4-D plots, as used already earlier to analyze double ionization [13, 14] and MPTI [15]. 4-D plots use a tetrahedral coordinate system. The distance of each tetrahedron corner to the opposite plane is 1. Each tetrahedron plane represents one of the final-state fragments. The front plane represents the electron emitted from the projectile, the bottom plane the electron ejected from the target, the right plane the projectile core, and the back plane the recoil ion. The distances of a given data point to the four planes are equal to the relative squared momenta $\pi_i = p_i^2 / \sum p_j^2$, where p_j is the momentum change of the j^{th} particle. Specifically, the momentum change of the recoil ion and the electron emitted from the target is equal to their momenta in the lab frame since they were initially at rest. The momentum change of the projectile fragments correspond to their momenta in the rest frame of the incoming projectile ion.

To illustrate how the 4-D plots should be read, consider, e.g., data points in the center of the tetrahedron, which are at equal distance to all four planes. This region represents equal momentum changes of all four particles, which means that MPTI proceeded through multiple interactions involving all four particles. Data points falling on the intersection lines between adjacent planes, which are labelled as 1-6 in Fig. 2 a), have at a distance of 0 to the intersecting planes thus corresponding to a zero momentum change of the corresponding particles. For example, at line 6 the planes for the target electron and the projectile electron intersect, for events near this line a momentum exchange mainly occurs between the cores of the two collision partners. We therefore associate such events with a binary interaction between the two cores, i.e. with elastic scattering. Likewise, we associate events at the other lines also with binary interactions between the remaining pairs of particles. However, as will be discussed later, the term "binary interaction" is somewhat misleading (because the role of the initial momenta is not accounted for) and we only use it for the sake of simplicity.

One disadvantage of 4-D plots is that it is not straightforward to generate them from calculated cross sections. The underlying problem is that in the chosen coordinate system the data features only a low degree of symmetry that could be taken advantage of in simplifying the integration of the FDCS which is necessary to compute the triple

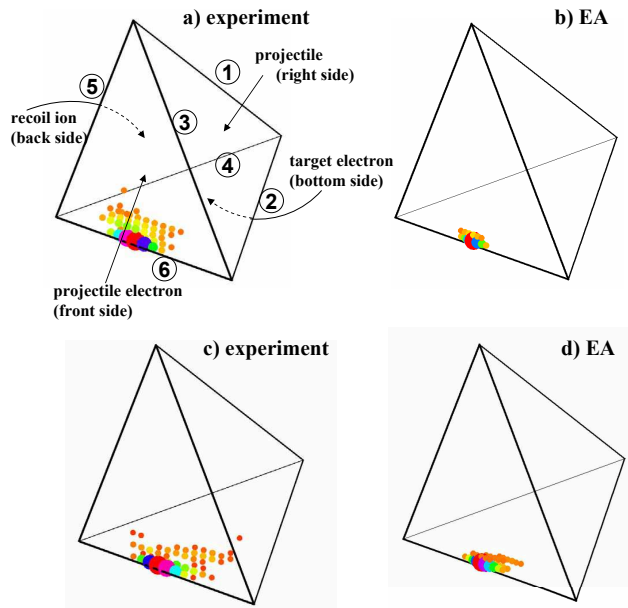


FIG. 2: (Color online) Four-particle Dalitz plots for MPI occurring in 1MeV/amu N^{4+} and N^{5+} + He collisions. The colour code along with the size of the points represent the number of events (the cross section) per unit volume of the Dalitz coordinates in a linear representation as indicated in the figure. a) N^{4+} + He experimental result, b) N^{4+} + He EA calculation result, c) N^{5+} + He experimental result, d) N^{5+} + He EA calculation result.

differential cross section represented by a 4-D plot¹. However, this problem could be solved by using a powerful tool, namely a Monte Carlo event generator (MCEG) techniques applied to atomic collisions [25]. There, an event file, similar to the data files of a multi-parameter coincidence measurement, is produced based on calculated FDCSs. With the MCEG technique the computation of 4-D plots has not only become feasible, but it also allows convoluting the theoretical cross sections with the experimental resolution, which is an extremely difficult (if not impossible) task for multi-parameter coincidence measurements using conventional methods. Furthermore, multiple scattering effects, not accounted for in the calculation, can be included retro-actively in the analysis of the theoretical event file using the MCEG technique.

The projectile velocity of 6.33 au corresponds to an electron kinetic energy of about 545eV. This energy is well above the anti-screening ionization threshold for N^{4+} + He (122.5 eV) while it is just barely below the threshold for N^{5+} + He (574 eV). As a result the e-e channel is expected to be strongly suppressed for the latter collision system, although it is kinematically still possible because of the initial momentum distribution of both active electrons in their initial state. On the other hand, for the N^{4+} projectiles one would expect the first-order contributions to be much more important than for N^{5+} .

Fig. 2 shows 4-D plots for MPI in 1MeV/amu N^{4+} (panel a) and N^{5+} + He collisions (panel c). The corresponding plots calculated with the EA model are shown in panels b) and d), respectively. The theoretical results are convoluted with elastic scattering of the two nuclei by the same method as reported by Schulz et al. [26]. The dominant feature in the data is a strong peak at intersection line 6. This shows that elastic scattering between the two cores is of high importance. Qualitatively, this can be explained by the relatively close collisions that mutual ionization on average requires (compared to e.g. single ionization). Therefore, the repulsive Coulomb force between the two cores is comparably large. This effect is less important for the electrons, due to the electron position distribution in the initial bound states. It should be noted that for N^{5+} the peak at line 6 is even more pronounced, which is consistent with the above analysis. Here, the electron ejected from the projectile originates from the K-shell so that the average impact parameter is reduced even further compared to N^{4+} , where the electron is initially predominantly in the L-shell. The results of the EA (panels b and d in Fig. 2), which includes both first- and higher-order contributions, reproduce the experimental data for both cases. Furthermore, the First Born Approximation (FBA) results (not shown in Fig.

[1] Although 4-D plots represent data as a function of the π_j of all four fragments only 3 π_j are independent because of the boundary condition $\sum \pi_j = 1$

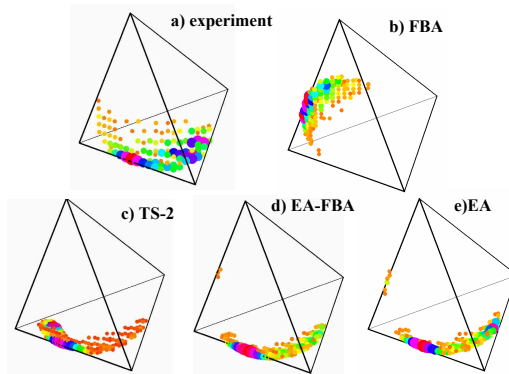


FIG. 3: (Color online) Longitudinal 4-D plots for MPTI occurring in 1MeV/amu $N^{5+} + He$ collisions. a) experimental result, b) FBA calculation result, c) TS-2 calculation result, d) EA-FBA calculation result, and e) EA calculation result.

2) are practically identical to the EA results. This similarity between the 4-D plots for N^{4+} and N^{5+} is due to the overwhelming dominance of elastic scattering between the cores, discussed above, which plays a similar role in the first- and higher-order processes. Therefore, these plots considering all components of the particle momentum vectors are not very suitable to identify and separate the first-order from the higher-order mechanisms.

The 4D-plots can also be generated for the momentum components along selected directions. For two reasons the longitudinal 4-D plots are of particular interest. First, in this direction the momentum transferred from the projectile to the target atom is basically determined by the projectile energy loss. Therefore, the longitudinal 4-D plots not only provide information about the momentum balance in the collision, but also about the kinetic energy balance. Second, elastic scattering, which overwhelms the 4-D plots for the three-dimensional case (see Fig. 2), plays no role in the longitudinal direction. In the force integral with respect to time, which determines the momentum transfer, the longitudinal components from the incoming and outgoing parts of the collision cancel each other to a very good approximation for the very small scattering angles realized in ion-atom collisions. The longitudinal 4-D plots should thus appear to be much more sensitive to the relative importance of the first- to higher-order contributions than the plots for the total (three-dimensional) momenta.

The longitudinal 4-D plots are shown for the 1MeV/amu $N^{5+} + He$ and 1MeV/amu $N^{4+} + He$ collision system in Fig. 3 and 4, respectively. This time the spectra of the two projectile charges look qualitatively very different. While for N^{5+} most of the events fall on the bottom plane representing small target electron momenta in the experimental data, the distribution for N^{4+} is more uniform with pronounced maxima occurring at intersection lines 4 and 5 and weaker maxima at lines 1, 2 and 6. Once again, this is qualitatively reproduced by our EA calculations, which now also yield different results for the two projectile charges.

The accumulation of events for the N^{5+} projectiles near the bottom plane, which represents a small momentum change of the target electron (Fig. 3a), is qualitatively predicted by the TS-2 calculation (Fig. 3c), which, as mentioned above, basically consists of a convolution of the cross sections for single ionization of the target and of the projectile. Essentially the same result is obtained with an EA calculation in which the first-order amplitude is subtracted (EA-FBA, Fig. 3d). In contrast, the FBA (Fig. 3b) predicts virtually no intensity at all near this plane. The large cross section for MPTI for small values of π_{te} for the target electron is thus a signature of higher-order processes. Finally, the experimental data are well reproduced by the EA calculation (Fig. 3e), which combines both first- and higher-order contributions. From the similarities between the experimental data and the TS-2 and the EA calculations it is clear that the higher-order processes dominate for this below anti-screening ionization threshold system.

For the N^{4+} projectiles, the interpretation of the comparison between experiment and theory is more complicated. The FBA predicts that the first order process results in a large intensity of events on the back plane, which represents small recoil ion momenta. The most pronounced peak structure on that plane occurs at line 1, which reflects the key role played by the electron-electron interaction in the first-order mechanism. The TS-2 calculation predicts most of the second order contributions to be on the bottom plane, which corresponds to small momenta of the target electron. Remarkably, the most pronounced peak in the experimental data (near the lower left corner of the tetrahedron) is reproduced by the TS-2 calculation. Again, similar results are obtained with the EA-FBA calculation. The EA results bear much more similarity with the FBA calculation than with the TS-2 results. More specifically, the main feature (the peak structure near line 1) in the FBA is still quite pronounced, while compared to the TS-2 calculation, the

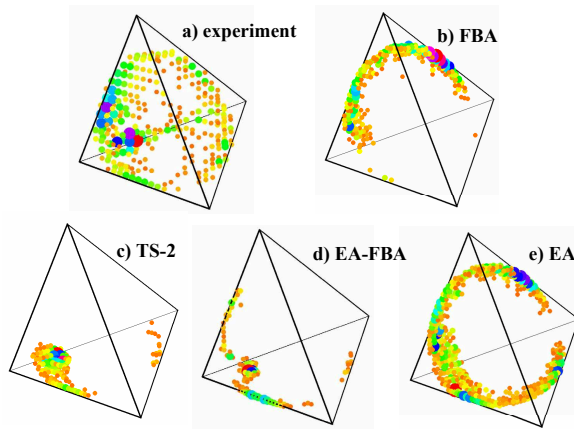


FIG. 4: (Color online) Longitudinal 4-D plots for MPTI occurring in 1MeV/amu $N^{4+} + He$ collisions. a) experimental result, b) FBA calculation result, c) TS-2 calculation result, d) EA-FBA calculation result, and e) EA calculation result.

dominant peak structure in the experimental data is strongly suppressed, as it is in the FBA. Evidently, the EA calculation predicts a predominance of first-order contributions because for projectile ionization from the 2s state of N^{4+} the projectile energy is well above the anti-screening ionization threshold.

However, the agreement between the EA model and the experimental data is rather poor, in sharp contrast to the N^{5+} case. In fact, the EA-FBA and TS-2 results yields better agreement in so far as they reproduce the most pronounced peak structure in the experimental data. Furthermore, the most prominent signature of the first-order process, a strong peak structure at line 1, is rather weak in the experimental data. These observations suggest that higher-order contributions are significantly more important than predicted by theory.

One question which arises from the comparison between experiment and theory is why the EA calculation is in nice qualitative agreement with the data for the N^{5+} projectiles, but not for the N^{4+} projectiles. A possible answer to this question may emerge by analyzing another feature of the EA calculations: for both projectile charge states they lead to a significant peak structure at line 2 (at the intersection between the bottom and the right plane), which is not seen in the FBA results² and it is at least strongly suppressed in the EA-FBA calculations. Since the EA amplitude is a coherent sum of the first-order (FBA) and higher-order amplitudes this peak structure must be due to constructive interference between both contributions. In the experimental data a pronounced maximum near that position is observed for the N^{5+} projectiles, but not for the N^{4+} projectiles, in other words, the interference predicted by theory is present in the former, but much weaker in the latter case.

In order to answer the question posed above we now need to understand why the presence or absence of interference depends on the projectile charge state. A possible explanation emerges from the transverse coherence length of the projectile. In fully quantum-mechanical calculations, like the EA approach, the projectile is described as a completely de-localized particle. However, very recently it was pointed out that more realistically the projectile should be represented by a wave packet with finite width, where the width is the transverse coherence length Δr [27]. In the same work, evidence was provided that Δr can have a large qualitative influence on collision cross sections. In the scattering angle dependence of ionization cross sections of molecular hydrogen, an interference pattern was present or absent depending on Δr . A similar situation may occur in the present study. For example, the cross sections could be affected by interference between two (or more) different impact parameters leading to the same scattering angle [28]. However, such an interference requires a coherent projectile beam, i.e. $\Delta r > \Delta b$, where Δb is the difference between the two interfering impact parameters. Since in MPTI for N^{5+} impact a K-shell electron has to be removed from the projectile, a typical Δb is much smaller than for N^{4+} impact, where an electron is mostly ejected from the L-shell of the projectile. As mentioned above in this experiment no collimating slit was used because the projectile beam is already reduced to a very small size through electron cooling in the storage ring. Under these circumstances it is difficult to estimate Δr , however, it is conceivable that the condition $\Delta r > \Delta b$ is realized for N^{5+} projectiles, but not for N^{4+} . In the EA calculation an infinite coherence length is assumed which is a better approximation for the N^{5+}

[2] It should be noted that the spectra are plotted with an offset in the cross sections in order to avoid the plots to be cluttered with data points. The FBA cross section near line 2 is not really 0, as suggested by Figs. 3 and 4, but it is very small.

projectiles than for N^{4+} . This could explain the significantly worse agreement with experiment for N^{4+} compared to N^{5+} impact.

V. CONCLUSION

We have studied mutual projectile and target ionization in 1MeV/amu N^{4+} and N^{5+} +He collisions in a kinematically complete experiment. The recoil ion and both active electrons were momentum analyzed using a reaction microscope specifically designed for operation in an ion storage ring. The momentum of the projectile after the collision was deduced from momentum conservation. Various theoretical models have been compared to the experimental result in the form of four-particle Dalitz plots, in which multiple differential cross sections as a function of all four particles are presented. The most important features of the experimental data are already reproduced by a simple TS-2 model, which describes the simultaneously but independently emission of the two electrons. Better agreement is achieved with the eikonal calculation result for the N^{5+} case. Noticeable discrepancies are observed in N^{4+} +He collisions between experimental data and our models. The experimental result shows significantly larger contributions from higher-order mechanisms than the eikonal calculation results. One possible explanation for these discrepancies is related to the interference between first- and higher-order processes predicted by theory. In the case of the N^{4+} projectiles the typical impact parameters could be larger than the width of the projectile wave packet, i.e. the transverse coherence length Δr . The interference predicted by theory, which unrealistically assume an infinite Δr , would then be artificial. In contrast, for the N^{5+} projectiles the typical impact parameters are much smaller because the electron is ejected from the K-shell, which could result in a real interference.

VI. ACKNOWLEDGEMENT

This work was supported by the Alliance Program of the Helmholtz Association (HA216/EMMI). MS acknowledges support by the National Science Foundation under grant no. 0969299

-
- [1] E. C. Montenegro, W. S. Melo, W. E. Meyerhof, and A. G. de Pinho, *Phys. Rev. Lett.* **69**, 3033 (1992).
 - [2] W. Wu, K. L. Wong, R. Ali, C. Y. Chen, C. L. Cocke, V. Frohne, J. P. Giese, M. Raphaelian, B. Walch, R. Dörner, et al., *Phys. Rev. Lett.* **72**, 3170 (1994).
 - [3] R. Dörner, V. Mergel, R. Ali, U. Buck, C. L. Cocke, K. Froschauer, O. Jagutzki, S. Lencinas, W. E. Meyerhof, S. Nüttgens, et al., *Phys. Rev. Lett.* **72**, 3166 (1994).
 - [4] H. Kollmus, R. Moshhammer, R. E. Olson, S. Hagmann, M. Schulz, and J. Ullrich, *Phys. Rev. Lett.* **88**, 103202 (2002).
 - [5] T. Ferger, D. Fischer, M. Schulz, R. Moshhammer, A. B. Voitkiv, B. Najjari, and J. Ullrich, *Phys. Rev. A* **72**, 062709 (2005).
 - [6] T. Ferger, M. Schulz, D. Fischer, B. Najjari, R. Moshhammer, and J. Ullrich, *Phys. Rev. A* **76**, 042708 (2007).
 - [7] A. C. F. Santos, G. M. Sigaud, W. S. Melo, M. M. Sant'Anna, and E. C. Montenegro, *Phys. Rev. A* **82**, 012704 (2010).
 - [8] G. K. H. Ehrhardt, K. Jung and P. Schlemmer, *Z. Phys. D.* **1**, 3 (1986).
 - [9] A. Lahmam-Bennani, *J. Phys. B: At. Mol. Opt. Phys.* **24**, 2401 (1991).
 - [10] J. H. McGuire, N. Stolterfoht, and P. R. Simony, *Phys. Rev. A* **24**, 97 (1981).
 - [11] R. H. Dalitz, *Philosophical Magazine* **44**, 1068 (1953).
 - [12] M. Schulz, R. Moshhammer, W. Schmitt, H. Kollmus, R. Mann, S. Hagmann, R. E. Olson, and J. Ullrich, *Phys. Rev. A* **61**, 022703 (2000).
 - [13] D. Fischer, M. Schulz, K. Schneider, M. F. Ciappina, T. Kirchner, A. Kelkar, S. Hagman, M. Grieser, K.-U. Kühnel, R. Moshhammer, et al., *Phys. Rev. A* **80**, 062703 (2009).
 - [14] M. Schulz, M. F. Ciappina, T. Kirchner, D. Fischer, R. Moshhammer, and J. Ullrich, *Phys. Rev. A* **79**, 042708 (2009).
 - [15] M. Schulz, D. Fischer, T. Ferger, R. Moshhammer, and J. Ullrich, *J. Phys. B: At. Mol. Opt. Phys.* **40**, 3091 (2007).
 - [16] E. Jaeschke, M. Blum, A. Friedrich, C. Geyer, M. Grieser, B. Holzer, H. W. Heyng, D. Habs, M. Jung, D. Kr?0?1mer, et al., *Part. Accel.* **32**, 97 (1990).
 - [17] M. Steck, G. Bisoffi, M. Blum, A. Friedrich, C. Geyer, M. Grieser, B. Holzer, E. Jaeschke, M. Jung, D. Kr?0?1mer, et al., *Nucl. Instr. and Meth. A* **287**, 324 (1990).
 - [18] G. Miersch, D. Habs, J. Kenntner, D. Schwalm, and A. Wolf, *Nucl. Instr. and Meth. A* **369**, 277 (1996).
 - [19] C. Cocke and R. E. Olson, *Phys. Rep.* **205**, 153 (1991).
 - [20] J. Ullrich, R. Moshhammer, R. Dörner, O. Jagutzki, V. Mergel, H. Schmidt-Böcking, and L. Spielberger, *J. Phys. B* **30**, 2917 (1997).
 - [21] R. Dörner, V. Mergel, O. Jagutzki, L. Spielberger, J. Ullrich, R. Moshhammer, and H. Schmidt-Böcking, *Physics Reports* **330**, 95 (2000).

- [22] J. Ullrich, R. Moshhammer, A. Dorn, R. Dörner, L. P. H. Schmidt, and H. Schmidt-Böcking, *Rep. Prog. Phys.* **66**, 1463 (2003).
- [23] A. B. Voitkiv and B. Najjari, *Journal of Physics B: Atomic, Molecular and Optical Physics* **38**, 3587 (2005).
- [24] A. B. Voitkiv and J. Ullrich, *Relativistic collisions of structured atomic particles* (Springer-Vellag Berlin Heidelberg, 2008).
- [25] M. Dürr, B. Najjari, M. Schulz, A. Dorn, R. Moshhammer, A. B. Voitkiv, and J. Ullrich, *Phys. Rev. A* **75**, 062708 (2007).
- [26] M. Schulz, M. Dürr, B. Najjari, R. Moshhammer, and J. Ullrich, *Phys. Rev. A* **76**, 032712 (2007).
- [27] K. N. Egodapitiya, S. Sharma, A. Hasan, A. C. Laforge, D. H. Madison, R. Moshhammer, and M. Schulz, *Phys. Rev. Lett.* **106**, 153202 (2011).
- [28] L. Sarkadi, *Phys. Rev. A* **82**, 052710 (2010).